# Noise-enhanced spatial-photonic Ising machine

Davide Pierangeli, Giulia Marcucci, Daniel Brunner, Claudio Conti

Research article

Davide Pierangeli*, Giulia Marcucci, Daniel Brunner and Claudio Conti

# Noise-enhanced spatial-photonic Ising machine

https://doi.org/10.1515/nanoph-2020-0119
Received February 14, 2020; accepted April 8, 2020; published online May 23, 2020

**Abstract:** Ising machines are novel computing devices for the energy minimization of Ising models. These combinatorial optimization problems are of paramount importance for science and technology, but remain difficult to tackle on large scale by conventional electronics. Recently, various photonics-based Ising machines demonstrated fast computing of a Ising ground state by data processing through multiple temporal or spatial optical channels. Experimental noise acts as a detrimental effect in many of these devices. On the contrary, here we demonstrate that an optimal noise level enhances the performance of spatial-photonic Ising machines on frustrated spin problems. By controlling the error rate at the detection, we introduce a noisy-feedback mechanism in an Ising machine based on spatial light modulation. We investigate the device performance on systems with hundreds of individually-addressable spins with all-to-all couplings and we found an increased success probability at a specific noise level. The optimal noise amplitude depends on graph properties and size, thus indicating an additional tunable parameter helpful in exploring complex energy landscapes and in avoiding getting stuck in local minima. Our experimental results identify noise as a potentially valuable resource for optical computing. This concept, which also holds in different nanophotonic neural networks, may be crucial in developing novel hardware with optics-enabled parallel architecture for large-scale optimizations.

**Keywords:** Ising machines; optical computing; optimization problems; spatial light modulation.

***Corresponding author: Davide Pierangeli**, Dipartimento di Fisica, Università di Roma "La Sapienza", 00185, Rome, Italy; Institute for Complex System, National Research Council (ISC-CNR), 00185, Rome, Italy, E-mail: davide.pierangeli@roma1.infn.it. https://orcid.org/0000-0002-5198-3743
**Giulia Marcucci and Claudio Conti:** Dipartimento di Fisica, Università di Roma "La Sapienza", 00185, Rome, Italy; Institute for Complex System, National Research Council (ISC-CNR), 00185, Rome, Italy, E-mail: giulia.marcucci@uniroma1.it (G. Marcucci), claudio.conti@uniroma1.it (C. Conti)
**Daniel Brunner:** Institut FEMTO-ST, Université Bourgogne Franche-Comté CNRS UMR 6174, Besançon, France, E-mail: daniel.brunner@femto-st.fr

## 1 Introduction

Solving large combinatorial problems is crucial for widespread applications in fields such as artificial intelligence, cryptography, biophysics, and complex networks. However, finding the optimal solution to many of these tasks causes the required resources to grow exponentially with the problem size, a reason why such problems are considered as computationally intractable for traditional computing architectures [1]. A promising approach to efficiently solve these problems is to recast them in terms of an Ising model [2, 3], which describes a system of classical interacting spins, and searching its ground state by an artificial network of spins evolving according to an Ising Hamiltonian. Ising machines are physical platforms made of electronic or photonic elements that can be programmed to encode Ising problems with known coupling values, and the ground state obtained after the system's relaxation provides the optimal solution. They have been realized in a variety of quantum and classical systems including cold atoms [4, 5], single photons [6, 7], superconducting [8, 9] and magnetic junctions [10], electromechanical [11] and CMOS circuits [12], polariton and photon condensates [13, 14], or lasers and nonlinear waves [15–17], but with practical difficulties in scalability, connectivity, or in engineering the spin interaction.

Photonic Ising machines encode the spin state in the phase or amplitude of the optical field. Realized photonically, such Ising machines hold the prospect of processing data in parallel at high speed through active optical components and hence be much faster than those based on other encoding schemes [18]. Various prototypes have recently been realized with sizes spanning from few to thousands of spins. In the class of photonic optimizers known as coherent Ising machines (CIMs), the nonlinear dynamics of time-multiplexed optical parametric oscillators [19–23], fiber lasers [24], or simple opto-electronic oscillators [25], is exploited to solve NP-hard optimization problems with notable performance [26]. CIMs are dissipative optical networks in which the ground-state search is performed in reverse direction by slowly raising the gain, according to a general non-equilibrium bifurcation mechanism that currently inspires novel algorithms and settings [27–37]. On the other hand, optimization platforms based on waveguides circuits [38, 39] and integrated nanophotonic processors

[40–43] operate as optical recurrent neural networks [44] converging to Ising energy minima.

Spatial-photonic Ising machines are a different class of optical devices for Ising problems that have been demonstrated very recently [45]. They make use of spatial light modulation for encoding an unprecedented number of spins [46] and the programmed Hamiltonian is optically evaluated by measuring the intensity distribution after propagation in free-space [45] or through nonlinear media [47]. These devices take advantage of optical vector-matrix multiplications and by the large pixel density of spatial light modulators (SLMs), thus enabling the implementation of large-scale neuromorphic computing [48–53].

Noise is an unavoidable ingredient in any hardware. In CIMs it represents one of the main error sources and can induce dynamics beyond the regime of Ising spins [55]. On the contrary, in recurrent algorithms and artificial neural networks for Ising problems, noise furnishes a finite effective temperature, and it is expected to facilitate and speed up convergence to the ground state if noise amplitude is adequately leveraged [40, 54]. The effect has been recently observed in a platform with few photonic spins and various competing interactions [41]. Noise-tolerant settings are especially important when scaling the device to solve systems with many units. Nevertheless, the impact of noise in large-scale photonic Ising machines remains mainly unexplored.

In the present article, we investigate the effect of experimental noise on a spatial-photonic Ising machine with hundreds of spins, proving the existence of an optimal noise level. The precise impact of noise depends on each problem's particular features. Specifically, we found that it enhances the machine's success probability on problems with both positive and negative interactions, while it is detrimental for models having only positive couplings. By providing a mechanism to escape from local minima, noise represents an additional parameter with beneficial properties for our optical computing device. Our findings demonstrate noise as a valuable resource in large-scale photonic computing.

# 2 Ising machine by spatial light modulation

In our Ising machine the spin variables are encoded on a coherent laser wavefront via binary values of the optical phase and processed by spatial light modulation [45]. As schematically illustrated in Figure 1(a), our optical setting employs an optical path in which an SLM encodes spins $\sigma_i = \pm 1$ by 0, $\pi$ phase delays over an amplitude-modulated beam. Linear interaction between spins occurs by interference on the detection plane and its strength is controlled by spatial modulation of the input intensity. The optical machine works via a measurement and feedback scheme. Once initialized to a given problem, feedback from the detected intensity allows the phase distribution on the SLM to converge towards a state minimizing an Ising Hamiltonian

$$H = -\sum_{ij} J_{ij}\sigma_i\sigma_j \tag{1}$$

with couplings $J_{ij} = \xi_i\xi_j\tilde{I}_T$, where $\xi_i$ is the amplitude illuminating the $i$th spin [45]. $\tilde{I}_T$ is the Fourier transform of a predetermined target image, and the difference between $I_T$ and the image detected on the camera is the cost function. At each machine iteration, we measure the intensity on the CCD modes [Figure 1(b)] and the spins are updated in order to minimize the cost function. Importantly, and other than for CIMs [20, 21, 25], our machine avoids electronically computing the energy as well as the field acting on each spin.

Due to the intrinsic noise of each experimental setup, the machine always behaves as coupled to a thermal bath. Noise therefore provides an effective temperature for the final spin ground state, as reported in Ref. [45]. Sources of noise come from intensity discretization and processing in each CCD mode, as well as from the imperfect spatial light modulation. As detailed below, we here control the noise level by means of a tunable error rate in the machine's measurement and feedback scheme.

## 2.1 Experimental setup and noisy-feedback method

The experimental device follows the setup illustrated in Figure 1(a). Light from a CW laser at $\lambda = 532$ nm is expanded and polarization controlled. The beam is first spatially modulated in amplitude and then in phase by a single reflective modulator (Holoeye LC-R 720, 1280 × 768 pixels, pixel pitch 20 × 20 $\mu$m). A section of the modulator operates in amplitude mode to generate the profiles $\xi_i$. A 4-f system then images this state on the second SLM section that performs binary phase modulation, which we realize with less than 10% residual intensity modulation. We select an active area of approximately 200 × 200 SLM pixels and divide it into $N$ addressable optical spins by grouping several pixels. Modulated light is spatially filtered using an holographic grating and focused by a $f = 500$ mm lens on a CCD camera. The intensity is detected on 18 × 18 spatial modes, where the signal in each mode is obtained averaging over 10 × 10 camera pixels, a size comparable with the spatial extent of a speckle grain.

The measured intensity pattern determines the feedback signal. At each machine cycle a single spin is randomly

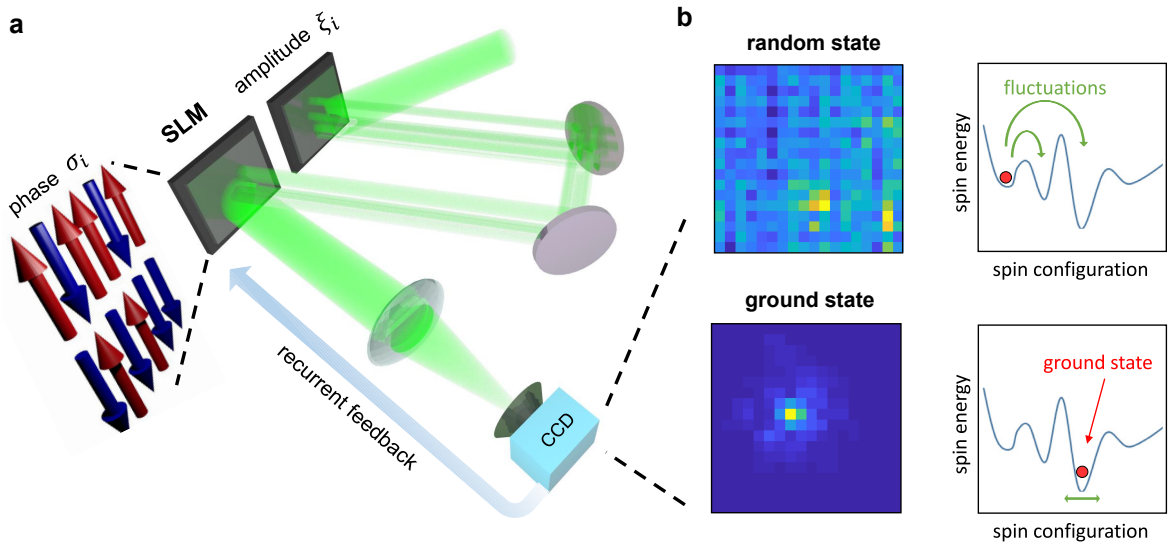


**Figure 1:** Photonic Ising machine by spatial light modulation. (a) The spins $\sigma_i = \pm 1$ are encoded by a spatial light modulator (SLM) into binary optical phases $\phi = 0, \pi$ in separated spatial points of the optical wavefront. Intensity modulation is employed to set the spin interaction via the amplitude distribution $\xi_i$. Recurrent feedback from the far-field camera allows evolution of the phase configuration towards the Ising ground state. (b) Intensity detected on the camera (CCD) modes for a random spin state and for the ground state of a ferromagnetic Ising model. Insets are illustrations of the corresponding spin state in energy landscape. Experimental fluctuations allow spontaneous changes in the spin configuration.

selected and flipped; the recorded image is compared with the reference $I_T$ on the same set of modes, and the spin state is updated to minimize the difference between the two images. Due to errors at the readout, there always exists a finite probability to update the spin configuration. The rate at which readout errors occur determines the noise level, which therefore is ultimately related to the magnitude of the intensity fluctuations on the detection plane. We exert control over the noise level by tuning the camera exposure time, where shorter exposure corresponds to larger error amplitudes. Fixing the CCD settings and analyzing the machine's behavior, we map the exposure time into a normalized noise level $\rho \in [0, 1]$, which indicates the probability at each iteration to measure a false decrease of the cost function and to erroneously flipping a spin. The minimum noise level available, $\rho = 0$, corresponds to faults in the feedback loop coming from spontaneous optical fluctuations in the setup.

## 2.2 Optimization with spontaneous noise

We first quantify the solutions found by our Ising machine for $\rho = 0$, a condition analogous to previously reported experiments [45]. We optically implement two different classes of Ising systems: mean-field and Mattis spin glasses. In a mean-field Ising model, also known as infinite-range Ising model, the spins are all-to-all coupled with the same positive interaction strength. We realize such coupling using a plane wave of constant amplitude $\xi_i = E_0$ and maximizing the intensity detected on a single CCD mode, such that $\tilde{I}_T = \mathrm{c}$, being c an arbitrary constant and $\tilde{J} = \mathrm{c}E_0^2$. In Mattis spin glasses the pairwise interaction is given as a product of two independent variables $J_{ij} \propto \xi_i \xi_j$ [56, 57]. In this case, since the couplings are both positive and negative, a minimal amount of noise introduces frustration [57]. In our spatial optical setting, pairs of negatively-coupled spins correspond to points of the optical field that give destructive interference on a fixed CCD mode [see bottom panel in Figure 2(d)]. Sparsity is implemented all-optically by decoupling a random subset of spins via amplitude modulation (i. e., $\xi_i = 0$ for blocks of spins). Since the interaction matrix is given in any case as a product of separate amplitude values, the sparse Ising Hamiltonian still maintains the form of a Mattis model.

Optical ground states found by the device for a mean-field system of $N = 100$ spins are reported in Figure 2(a–c). The evolution of a spin configuration initialized to a random distribution is shown in Figure 2(b) for a single machine run; after thousand iterations, a low-temperature ferromagnetic state is measured. The energy probability distribution of these ground states is reported in Figure 2(c); a peak close to the known minimum energy value [red line in Figure 2(c)] indicates that ground states of the Ising Hamiltonian are successfully found. In Figure 2(d)

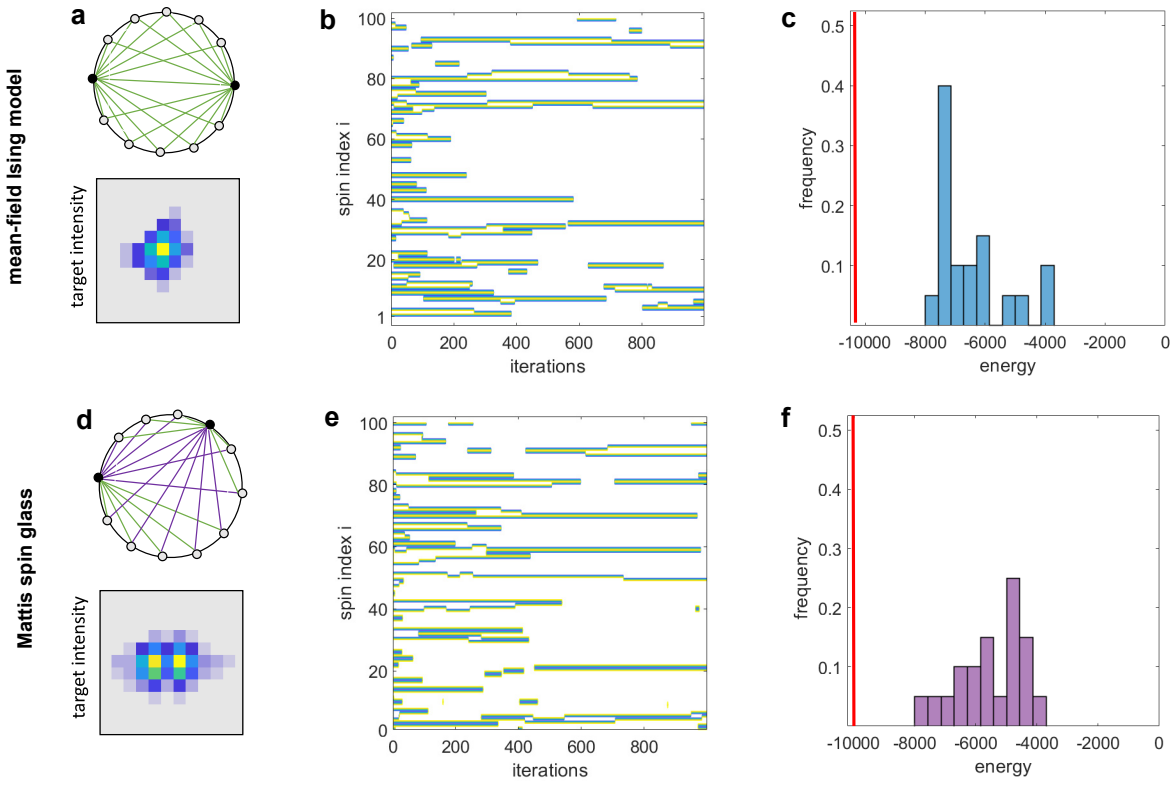


**Figure 2:** Ising machine's ground states without noise control. (a–c) Results for ferromagnetic and (d–f) frustrated models with 100 spins ($\rho = 0$). Problem graphs for (a) mean-field (infinite-range) Ising model and (d) Mattis spin glass with positive and negative couplings. For clarity, only links starting from the two black nodes are drawn. Insets show the corresponding target images $I_T$. (b, e) Contour maps showing the evolution of the spin configuration during a single run of the machine (green regions are domain walls). (c, f) Normalized histograms of the ground-state energy obtained for the instances in (a) and (d), respectively. The red lines in (c) and (f) indicate the minimum energy known from exact solution of the models.

we show the graph for a Mattis spin glass instance along with the corresponding target image. In agreement with the programmed Hamiltonian [57], the spin evolution in Figure 2(e) exhibits the formation of two domains with opposite magnetization and equal size. However, from the ground-state energies in Figure 2(f), we observe a reduced ability of the machine in solving such frustrated models. As we demonstrate hereafter, increasing the noise level is an effective way to improve the machine performance on problems affected by trapping in local energy minima.

## 3 Effect of the noise level on the Ising machine performance

To introduce controllable noise, we exploit the detection process previously described. The Ising machine is made to operate under different noise levels. To quantify the performance when the setup is initialized to different parameters, we use two distinct and complementary quantities: the success probability $p_s$ and the Hamming distance $h$. To evaluate the success of the computation, we consider the correlation between the measured spin configuration and the known optimal solution, being $C = \pm 1$ for the zero-temperature spin system in the lowest energy state [57]. A machine run is defined as successful if its final state gives $|C| > a$, being $a$ any fixed accuracy; the success probability $p_s$ is the fraction of repeated experiments with random initial conditions that converged successfully. The Hamming distance is a metric used in information theory. Here, $h$ indicates the number of units (spins) that need to be inverted to reach the minimum energy configuration [9]. We would like to point out that using this quantity to characterize the quality of Ising machines is significantly more accurate than the ground-state energy. In fact, spin configurations very far from the known solution can still have energies comparable with the optimal one.

Figure 3 illustrates the performance of the spatial-photonic Ising machine as we vary the noise level. For the

infinite-range Ising model, we found a success probability that decays as noise increases, a behavior independent of the selected accuracy [Figure 3(a)]. The measured $h$ in Figure 3(b) has a growing trend, thus indicating that for emulating such Hamiltonians the best performance is obtained for minimum noise. A completely different picture emerges when solving frustrated Ising models. As shown in Figure 3(c) for dense Mattis spin glass instances, the low success probability observed under spontaneous noise rapidly increases as additional fluctuations are introduced. $p_s$ has a maximum value and then decays to zero for large noise levels. Moreover, the mean Hamming distance as a function of the noise level exhibits a pronounced minimum [Figure 3(d)], which indicates an optimal noise level, $\rho_{opt} \approx 0.05$. A similar behavior is found on sparse Mattis spin glasses, as reported in Figure 3(e–f), with $\rho_{opt} \approx 0.07$. This demonstrates that an optimal noise level promotes the exploration of energy landscapes with many minima during optimization on the optical platform.

## 3.1 Scaling of the optimal noise level

We investigate how the noise-enhanced machine operation depends on the system size. While keeping the SLM's active area constant, we vary the total number of spins and, for each system size $N$, we perform the experiments at different noise levels. The results obtained on dense Mattis spin glasses are shown in Figure 4. We observe an optimal noise level that significantly depends on the spin number, with values that grow and saturate as the system size increases. For small-scale systems ($N$ = 16) additional noise yields only limited advantages due to finite size effects and the small number of frustrated configurations. However, a constant optimal level $\rho_{opt} \approx 0.07$ enhances the optimization for large scale Hamiltonians. This specific value is not a general recipe to improve the Ising machine, but guarantees improved performance on specific problem graphs in our setup. Ising instances with distinct properties (graph type, connection density etc.) would have diverse optimal levels, having landscapes with different features. These

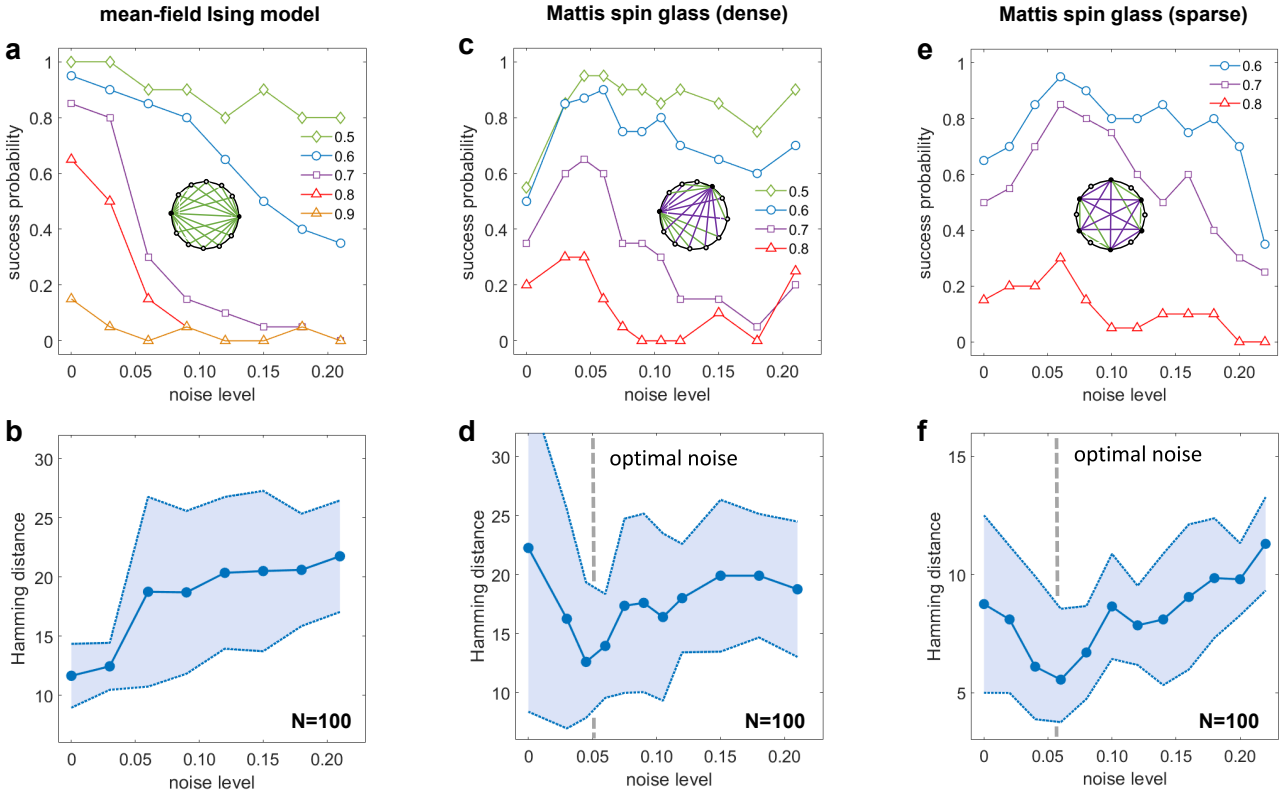


**Figure 3:** Optimal noise level in spatial-photonic Ising machines. (a, c, e) Success probability and (b, d, f) mean Hamming distance varying the noise level for various $N$ = 100 Ising models: (a–b) mean-field Ising model, (c–d) dense and (e–f) sparse Mattis spin glasses. The problem graphs are inset. Different colors in (a, c, e) indicate data obtained at the specified accuracy level. Shaded regions indicate statistical error intervals. The existence of an optimal noise level for frustrated models is signaled by a minimum in the Hamming distance and a corresponding maximum in the success probability [dotted line in (d) and (f)].

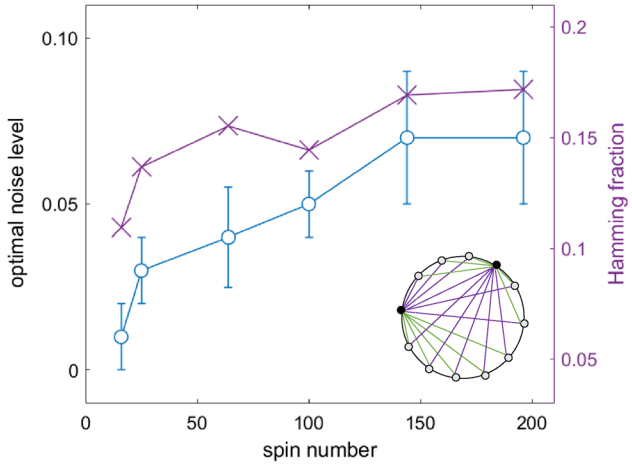


**Figure 4:** Scaling properties. Optimal noise level (blue circles) as a function of the number of spins for dense Mattis spin glasses (inset graph). Purple dots indicate the measured Hamming fraction ($h/N$) for various system sizes.

findings establish the noise level as a hyperparameter of the photonic computing device.

Another important fact is that residual errors do not increase rapidly with $N$. To prove this property, Figure 4 shows the Hamming fraction $h/N$ (i. e., the mean Hamming distance normalized to the spin number) as a function of $N$. Residual errors shows a sublinear increase with minor oscillations as $N$ varies. This preliminary evidence suggest a smooth dependence of the machine accuracy on the system size, although larger systems naturally require more machine iterations to converge to their ground state. According to thermodynamic considerations, this is consistent with the presence of an effective thermal bath for the spin state. It suggests that lowering the effective temperature of the machine by improving the experimental setup can lead to larger ground-state probabilities even for large-scale models.

## 4 Conclusions

Understanding the role of noise in optical Ising machines and neuromorphic devices is crucial for their application to large-scale computational tasks. In particular, noise-tolerant settings are attractive candidates for developing unconventional computing architectures. We have reported the first evidence that spatial-photonic Ising machines can take advantage of noise in solving large-scale optimization problems. Devices based on spatial light modulation are scalable to larger sizes and can potentially host systems consisting of millions of spins. In particular, our computing setting can exploit the potential of nanophotonic light-modulation devices. Tunable dielectric metasurfaces, which allow to control both phase and polarization of the optical wavefront with subwavelength spatial resolution [58], can act as high-density phase modulators, enabling the integration of SLM-based Ising machines on a photonic chip. For example, more than $10^6$ optical spins over square millimeter could be obtained through the development of novel SLM technologies that integrate nanoantennas into liquid crystal cells [59]. Alternative nanophotonic platforms that employ electro-optic microcavity arrays would allow to achieve high fill factors along with phase-only modulation at GHz speeds [60]. At present, the iteration time of our Ising machine can be reduced to a few milliseconds by exploiting the most recent microelectromechanical SLM technologies [61, 62]. Spatial-photonic Ising machines are thus a promising approach for large-scale ultra-fast optical computing.

In conclusion, introducing a noisy-feedback mechanism in an SLM-based scheme, we have demonstrated the existence of an optimal noise level enhancing the machine performance on frustrated Ising models. Noise can hence be exploited as a tunable parameter to improve the exploration of energy landscapes with many minima, an interesting property that has been identified also in neural-network-based nanophotonic Ising samplers [40, 41]. Photonic Ising machines with controllable noise represent a route to realize photonic simulations of phase transition and finite-temperature phenomena. Our results show that noise is a valuable resource for optical computing, opening important possibilities for realizing classical and quantum annealing.

**Acknowledgments:** We acknowledge funding from Sapienza Ateneo, SAPIExcellence 2019 (SPIM project), QuantERA ERA-NET Co-fund (Grant No. 731473, project QUOMPLEX), PRIN PELM 2017 and H2020 PhoQus project (Grant No. 820392). We thank Mr. MD Deen Islam for technical support in the laboratory.

## References

[1] J. Hromkovič, *Algorithmics for Hard Problems: Introduction to Combinatorial Optimization, Randomization, Approximation, and Heuristics*. Berlin Heidelberg, Springer, 2013.

[2] F. Barahona, "On the computational complexity of Ising spin glass models," *J. Phys. Math. Gen.*, vol. 15, p. 3241, 1982, https://doi.org/10.1088/0305-4470/15/10/028.

[3] A. Lucas, "Ising formulations of many NP problems," *Front. Phys.*, vol. 2, p. 1, 2014, https://doi.org/10.3389/fphy.2014.00005.

[4] K. Kim, M. S. Chang, S. Korenblit, et al., "Quantum simulation of frustrated Ising spins with trapped ions," *Nature*, vol. 465, p. 590, 2010, https://doi.org/10.1038/nature09071.
[5] J. Simon, W. S. Bakr, R. Ma, M. E. Tai, P. M. Preiss, and M. Greiner, "Quantum simulation of antiferromagnetic spin chains in an optical lattice," *Nature*, vol. 472, p. 307, 2011, https://doi.org/10.1038/nature09994.
[6] X. Ma, B. Dakic, W. Naylor, A. Zeilinger, and P. Walther, "Quantum simulation of the wavefunction to probe frustrated Heisenberg spin systems," *Nat. Phys.*, vol. 7, p. 399, 2011, https://doi.org/10.1038/nphys1919.
[7] I. Pitsios, L. Banchi, A. S. Rab, et al., "Photonic simulation of entanglement growth and engineering after a spin chain quench," *Nat. Commun.*, vol. 8, p. 1569, 2017, https://doi.org/10.1038/s41467-017-01589-y.
[8] M. W. Johnson, M. H. S. Amin, S. Gildert, et al., "Quantum annealing with manufactured spins," *Nature*, vol. 473, p. 194, 2011, https://doi.org/10.1038/nature10012.
[9] S. Boixo, T. F. Rønnow, S. V. Isakov, et al., "Evidence for quantum annealing with more than one hundred qubits," *Nat. Phys.*, vol. 10, p. 214, 2014, https://doi.org/10.1038/nphys2900.
[10] W. A. Borders, A. Z. Pervaiz, S.Fukami, K. Y. Camsari, H. Ohno, and S. Datta, "Integer factorization using stochastic magnetic tunnel junctions," *Nature*, vol. 573, p. 390, 2019, https://doi.org/10.1038/s41586-019-1557-9.
[11] I. Mahboob, H. Okamoto, and H. Yamaguchi, "An electromechanical Ising Hamiltonian," *Sci. Adv.*, vol. 2, p. e1600236, 2016, https://doi.org/10.1126/sciadv.1600236.
[12] M. Yamaoka, C. Yoshimura, M. Hayashi, T. Okuyama, H. Aoki, and H. Mizuno, "A 20k-spin Ising chip to solve combinatorial optimization problems with CMOS annealing," *IEEE J. Solid State Circ.*, vol. 51, p. 303, 2015, https://doi.org/10.1109/jssc.2015.2498601.
[13] N.G. Berloff, M. Silva, K. Kalinin, et al., "Realizing the classical XY Hamiltonian in polariton simulators," *Nat. Mater.*, vol. 16, p. 1120, 2017, https://doi.org/10.1038/nmat4971.
[14] D. Dung, C. Kurtscheid, T. Damm, et al., "Variable potentials for thermalized light and coupled condensates," *Nat. Photon.*, vol. 11, p. 565, 2017, https://doi.org/10.1038/nphoton.2017.139.
[15] N. Ghofraniha, I. Viola, F. Di Maria, et al., "Experimental evidence of replica symmetry breaking in random lasers," *Nat. Commun.*, vol. 6, p. 6058, 2015, https://doi.org/10.1038/ncomms7058.
[16] M. Nixon, E. Ronen, A. A. Friesem, and N. Davidson, "Observing geometric frustration with thousands of coupled lasers," *Phys. Rev. Lett.*, vol. 110, 2013, Art no. 184102, https://doi.org/10.1103/physrevlett.110.184102.
[17] D. Pierangeli, A. Tavani, F. Di Mei, A. J. Agranat, C. Conti, and E. DelRe, "Observation of replica symmetry breaking in disordered nonlinear wave propagation," *Nat. Commun.*, vol. 8, p. 1501, 2017, https://doi.org/10.1038/s41467-017-01612-2.
[18] D. Brunner, M. C. Soriano, C. Mirasso, and I. Fischer, "Parallel photonic information processing at gigabyte per second data rates using transient states," *Nat. Commun.*, vol. 4, p. 1364, 2013, https://doi.org/10.1038/ncomms2368.
[19] A. Marandi, Z. Wang, K. Takata, R. L. Byer, and Y. Yamamoto, "Network of time-multiplexed optical parametric oscillators as coherent Ising machine," *Nat. Photon.*, vol. 8, p. 937, 2014, https://doi.org/10.1038/nphoton.2014.249.
[20] P. L. McMahon, A. Marandi, Y. Haribara, et al., "A fully-programmable 100-spin coherent Ising machine with all-to-all connections," *Science*, vol. 354, p. 614, 2016, https://doi.org/10.1126/science.aah5178.
[21] T. Inagaki, Y. Haribara, K. Igarashi, et al., "A coherent Ising machine for 2000-node optimization problems," *Science*, vol. 354, p. 603, 2016, https://doi.org/10.1126/science.aah4243.
[22] T. Inagaki, K. Inaba, R. Hamerly, K. Inoue, Y. Yamamoto, and H. Takesue, "Large-scale Ising spin network based on degenerate optical parametric oscillators," *Nat. Photon.*, vol. 10, p. 415, 2016, https://doi.org/10.1038/nphoton.2016.68.
[23] Y. Takeda, S. Tamate, Y. Yamamoto, H. Takesue, T. Inagaki, and S. Utsunomiya, "Boltzmann sampling for an XY model using a non-degenerate optical parametric oscillator network," *Quant. Sci. Technol.*, vol. 3, 2018, Art no. 014004, https://doi.org/10.1088/2058-9565/aa923b.
[24] M. Babaeian, D. T. Nguyen, V. Demir, et al., "A single shot coherent Ising machine based on a network of injection-locked multicore fiber lasers," *Nat. Commun.*, vol. 10, p. 3516, 2019, https://doi.org/10.1038/s41467-019-11548-4.
[25] F. Böhm, G. Verschaffelt, and G. Van der Sande, "A poor man's coherent Ising machine based on opto-electronic feedback systems for solving optimization problems," *Nat. Commun.*, vol. 10, p. 3538, 2019, https://doi.org/10.1038/s41467-019-11484-3.
[26] R. Hamerly, T. Inagaki, P. L. McMahon, et al., "Experimental investigation of performance differences between coherent Ising machines and a quantum annealer," *Sci. Adv.*, vol. 5, 2019, Art no. eaau0823, https://doi.org/10.1126/sciadv.aau0823.
[27] H. Goto, K. Tatsumura, and A. R. Dixon, "Combinatorial optimization by simulating adiabatic bifurcations in nonlinear Hamiltonian systems," *Sci. Adv.*, vol. 5, 2019, Art no. eaav2372, https://doi.org/10.1126/sciadv.aav2372.
[28] K. P. Kalinin and N. G. Berloff, "Global optimization of spin Hamiltonians with gain-dissipative systems," *Sci. Rep.*, vol. 8, p. 17791, 2018, https://doi.org/10.1038/s41598-018-35416-1.
[29] S. Puri, C. K. Andersen, A. L. Grimsmo, and A. Blais, "Quantum annealing with all-to-all connected nonlinear oscillators," *Nat. Commun.*, vol. 8, p. 15785, 2017, https://doi.org/10.1038/ncomms15785.
[30] E. S. Tiunov, A. E. Ulanov, and A. I. Lvovsky, "Annealing by simulating the coherent Ising machine," *Opt. Express*, vol. 27, p. 10288, 2019, https://doi.org/10.1364/oe.27.010288.
[31] W. R. Clements, J. J. Renema, Y. H. Wen, H. M. Chrzanowski, W. S. Kolthammer, and I. A. Walmsley, "Gaussian optical Ising machines," *Phys. Rev.*, vol. 96, 2017, Art no. 043850, https://doi.org/10.1103/physreva.96.043850.
[32] F. Böhm, T. Inagaki, K. Inaba, et al., "Understanding dynamics of coherent Ising machines through simulation of large-scale 2D Ising models," *Nat. Commun.*, vol. 9, p. 5020, 2018, https://doi.org/10.1038/s41467-018-07328-1.
[33] K. P. Kalinin and N. G. Berloff, "Simulating Ising and n-state planar potts models and external fields with nonequilibrium condensates," *Phys. Rev. Lett.*, vol. 121, 2018, Art no. 235302, https://doi.org/10.1103/physrevlett.121.235302.
[34] T. Leleu, Y. Yamamoto, P. L. McMahon, and K. Aihara, "Destabilization of local minima in analog spin systems by correction of amplitude heterogeneity," *Phys. Rev. Lett.*, vol. 122, 2019, Art no. 040607, https://doi.org/10.1103/physrevlett.122.040607.

[35] L. Bello, M. Calvanese Strinati, E. G. Dalla Torre, and A. Pe'er, "Persistent coherent beating in coupled parametric oscillators," *Phys. Rev. Lett.*, vol. 123, 2019, Art no. 083901, https://doi.org/10.1103/physrevlett.123.083901.

[36] J. Chou, S. Bramhavar, S. Ghosh, and W. Herzog, "Analog coupled oscillator based weighted Ising machine," *Sci. Rep.*, vol. 9, p. 14786, 2019, https://doi.org/10.1038/s41598-019-49699-5.

[37] C. Tradonsky, I. Gershenzon, V. Pal, et al., "Rapid laser solver for the phase retrieval problem," *Sci. Adv.*, vol. 5, 2019, Art no. eaax4530, https://doi.org/10.1126/sciadv.aax4530.

[38] K. Wu, J. García de Abajo, C. Soci, P. P. Shum, and N. I. Zheludev, "An optical fiber network oracle for NP-complete problems," *Light Sci. Appl.*, vol. 3, p. e147, 2014, https://doi.org/10.1038/lsa.2014.28.

[39] M. R. Vázquez, V. Bharadwaj, B. Sotillo, et al., "Optical NP problem solver on laser-written waveguide platform," *Opt. Express*, vol. 26, p. 702, 2018, https://doi.org/10.1364/OE.26.000702.

[40] C. Roques-Carmes, Y. Shen, C. Zanoci, et al., "Heuristic recurrent algorithms for photonic Ising machines," *Nat. Commun.*, vol. 11, p. 249, 2020, https://doi.org/10.1038/s41467-019-14096-z.

[41] M. Prabhu, C. Roques-Carmes, Y. Shen, et al., A recurrent Ising machine in a photonic integrated circuit, arXiv:1909. 13877v1, 2019, https://doi.org/10.1364/optica.386613.

[42] Y. Shen, N. C. Harris, S. Skirlo, et al., "Deep learning with coherent nanophotonic circuits," *Nat. Photon.*, vol. 11, p. 441, 2017, https://doi.org/10.1038/nphoton.2017.93.

[43] N. C. Harris, J. Carolan, D. Bunandar, et al., "Linear programmable nanophotonic processors," *Optica*, vol. 5, p. 1623, 2018, https://doi.org/10.1364/optica.5.001623.

[44] J. Bueno, S. Maktoobi, L. Froehly, et al., "Reinforcement learning in a large-scale photonic recurrent neural network," *Optica*, vol. 5, p. 756, 2018, https://doi.org/10.1364/optica.5.000756.

[45] D. Pierangeli, G. Marcucci, and C. Conti, "Large-scale photonic Ising machine by spatial light modulation," *Phys. Rev. Lett.*, vol. 122, 2019, Art no. 213902, https://doi.org/10.1103/physrevlett.122.213902.

[46] C. Roques-Carmes, and M. Soljačić, "Photonic Ising machines go big," *Physics*, vol. 12, 2019, https://doi.org/10.1103/physics.12.61.

[47] S. Kumar, H. Zhang, and Y. P. Huang, "Large-scale Ising emulation with four-body interaction and all-to-all connection," arXiv:2001. 05680v1, 2020.

[48] R. Hamerly, L. Bernstein, A. Sludds, M. Soljačić, and D. Englund, "Large-scale optical neural networks based on photoelectric multiplication," *Phys. Rev. X*, vol. 9, 2019, Art no. 021032, https://doi.org/10.1103/PhysRevX.9.021032.

[49] Y. Zuo, B. Li, Y. Zhao, et al., "All-optical neural network with nonlinear activation functions," *Optica*, vol. 6, p. 1132, 2019, https://doi.org/10.1364/optica.6.001132.

[50] A. Saade, F. Caltagirone, I. Carron, et al., "Random projections through multiple optical scattering: Approximating kernels at the speed of light," *ICASSP, IEEE Int. Conf. Acoust. Speech Signal Process.*, p. 6215, 2106, https://doi.org/10.1109/icassp.2016.7472872.

[51] J. Dong, M. Rafayelyan, F. Krzakala, and S. Gigan, "Optical reservoir computing using multiple light scattering for chaotic systems prediction," *IEEE J. Sel. Top. Quant. Electron.*, vol. 26, pp. 1–12, 2020, https://doi.org/10.1109/jstqe.2019.2936281.

[52] P. del Hougne and G. Lerosey, "Leveraging chaos for wave-based analog computation: Demonstration with indoor wireless communication signals," *Phys. Rev. X*, vol. 8, 2018, Art no. 041037, https://doi.org/10.1103/PhysRevX.8.041037.

[53] M. W. Matthès, P. Del Hougne, J. De Rosny, G. Lerosey, and S. M. Popoff, "Optical complex media as universal reconfigurable linear operators," *Optica*, vol. 6, p. 465, 2019, https://doi.org/10.1364/optica.6.000465.

[54] F. Cai, S. Kumar, T. Van Vaerenbergh, et al., Harnessing intrinsic noise in memristor hopfield neural networks for combinatorial optimization, arXiv:1903, 11194v2, 2019.

[55] M. C. Strinati, L. Bello, A. Pe'er, and E. G. Dalla Torre, "Theory of coupled parametric oscillators beyond coupled Ising spins," *Phys. Rev.*, vol. 100, 2019, Art no. 023835, https://doi.org/10.1103/physreva.100.023835.

[56] D. C. Mattis, "Solvable spin systems with random interactions, *Phys. Lett. A*, vol. 56, p. 421, 1976.

[57] H. Nishimori, *Statistical Physics of Spin Glasses and Information Processing: An Introduction, Vol. 111*. Oxford: Clarendon Press, 2001.

[58] S. M. Kamalia, E. Arbabia, A. Arbabi and A. Faraon, "A review of dielectric optical metasurfaces for wavefront control," *Nanophotonics*, vol. 7, p. 1041, 2018, https://doi.org/10.1515/nanoph-2017-0129.

[59] S. Q. Li, X. Xu, R. M. Veetil, V. Valuckas, R. Paniagua-Domínguez, and A. I. Kuznetsov, "Phase-only transmissive spatial light modulator based on tunable dielectric metasurface," *Science*, vol. 364, p. 1087, 2019, https://doi.org/10.1126/science.aaw6747.

[60] C. Peng, R. Hamerly, M. Soltani, and D. R. Englund, "Design of high-speed phase-only spatial light modulators with two-dimensional tunable microcavity arrays," *Opt. Express*, vol. 27, p. 30669, 2019, https://doi.org/10.1364/OE.27.030669.

[61] B. Blochet, L. Bourdieu, and S. Gigan, "Focusing light through dynamical samples using fast continuous wavefront optimization," *Opt. Lett.*, vol. 42, p. 4994, 2017, https://doi.org/10.1364/OL.42.004994.

[62] O. Tzang, E. Niv, S. Singh, S. Labouesse, G. Myatt, and R. Piestun, "Wavefront shaping in complex media with a 350 KHz modulator via a 1D-to-2D transform," *Nat. Photon.*, vol. 13, p. 788, 2019, https://doi.org/10.1038/s41566-019-0503-6.